

# The Tutorial: $S$ Transform

Yu-Hsiang Wang (王昱翔)

E-mail: r98942059@ntu.edu.tw

Graduate Institute of Communication Engineering  
National Taiwan University, Taipei, Taiwan, ROC

## Abstract

The  $S$  transform is variable window of short time Fourier transform (STFT) or an extension of wavelet transform (WT). It is based on a scalable localizing Gaussian window and supplies the frequency dependent resolution. In this tutorial, we introduce the fundamental function of  $S$  transform and the generalized  $S$  transform. Furthermore, we present some applications of  $S$  transform: seismogram analysis, analysis of engine induction noise in acceleration, and power quality analysis. Then compare the result of  $S$  transform with other time-frequency analysis and exhibit some different windows of  $S$  transform.

## 1. Introduction

Although the Fourier transform of the entire time series does contain information about the spectral components in time series, it cannot detect the time distribution of different frequency, so for a large class of practical applications, the Fourier transform is unsuitable. So the time-frequency analysis is proposed and applied in some special situations. The STFT is most often used. But the STFT cannot track the signal dynamics properly for non-stationary signal due to the limitations of fixed window width. The WT is good at extracting information from both time and frequency domains. However, the WT is sensitive to noise. The  $S$  transform was proposed by Stockwell and his coworkers in 1996. The properties of  $S$  transform are that it has a frequency dependent resolution of time-frequency domain and entirely refer to local phase information. For example, in the beginning of earthquake, the spectral components of the P-wave clearly have a strong dependence on time. So we need the generalized  $S$  transform to emphasize the time resolution in the beginning time and the frequency resolution in the later of beginning time. Based on different purposes, we can apply different window of  $S$  transform. For example, we will introduce the Gaussian window, the bi-Gaussian window, and the hyperbolic window.

In chapter 2, we introduce the fundamental mathematical formula of the  $S$

transform, its relation with the STFT and the WT, its properties, and the simulation result with  $S$  transform and other time-frequency analysis implement. In chapter 3, we present the generalized  $S$  transform and illustrate the properties of the windows. After chapter 4, we will show some applications with different windows and analyze the result of those applications.

## 2. The $S$ Transform

There are some different methods of achieving the  $S$  transform. We introduce the relationship between STFT and  $S$  transform. And the type of deriving the  $S$  transform from the "phase correction" of the CWT here, learned from [1].

### 2.1 The Continuous $S$ Transform

#### 2.1.1 Relationship between $S$ Transform and STFT

The STFT of signal  $h(t)$  is defined as

$$STFT(\tau, f) = \int_{-\infty}^{\infty} h(t)g(\tau - t)e^{-j2\pi ft} dt \quad (2.1)$$

where  $\tau$  and  $f$  denote the time of spectral localization and Fourier frequency, respectively, and  $g(t)$  denote a window function.

The  $S$  transform can derive from (2.1) by replacing the window function  $g(t)$  with the Gaussian function, shown as

$$g(t) = \frac{|f|}{\sqrt{2\pi}} e^{-\frac{t^2 f^2}{2}}. \quad (2.2)$$

Then the  $S$  transform is defined as

$$S(\tau, f) = STFT(\tau, f) = \int_{-\infty}^{\infty} h(t) \frac{|f|}{\sqrt{2\pi}} e^{-\frac{(\tau - t)^2 f^2}{2}} e^{-j2\pi ft} dt. \quad (2.3)$$

So we can say that the  $S$  transform is a special case of STFT with Gaussian window function. If the window of  $S$  transform is wider in time domain,  $S$  transform can provide better frequency resolution for lower frequency. While the window is narrower, it can provide better time resolution for higher frequency.

## 2.1.1 Relationship between $S$ Transform and CWT

The continuous-time expression of the CWT is

$$W(\tau, d) = \int_{-\infty}^{\infty} h(t) \omega(t - \tau, d) dt \quad (2.4)$$

where  $t$  denotes time,  $h(t)$  denotes a function of time,  $\tau$  denotes the time of spectral localization,  $d$  denotes the "width" of the wavelet  $w(t, d)$  and thus it controls the resolution, and  $w(t, d)$  denotes a scaled copy of the fundamental mother wavelet. Along with (2.4), there has a constraint of the mother wavelet  $w(t, d)$  that  $w(t, d)$  must have zero mean.

Then the  $S$  transform is defined as a CWT with a specific mother wavelet multiplied by the phase factor

$$S(\tau, f) = e^{-j2\pi f \tau} W(\tau, d) \quad (2.5)$$

where the mother wavelet is defined as

$$\omega(t, f) = \frac{|f|}{\sqrt{2\pi}} e^{-\frac{t^2 f^2}{2}} e^{-j2\pi f t} . \quad (2.6)$$

Note that the factor  $d$  is the inverse of the frequency  $f$ .

However the mother wavelet in (2.6) does not satisfy the property of zero mean, (2.5) is not absolutely a CWT. In other words, the  $S$  transform is not equal to CWT, it is given by

$$S(\tau, f) = \int_{-\infty}^{\infty} h(t) \frac{|f|}{\sqrt{2\pi}} e^{-\frac{(\tau-t)^2 f^2}{2}} e^{-j2\pi f t} dt . \quad (2.7)$$

If the  $S$  transform is a representation of the local spectrum, we can show that the relation between the  $S$  transform and Fourier transform as

$$\int_{-\infty}^{\infty} S(\tau, f) d\tau = H(f) \quad (2.8)$$

where  $H(f)$  is the Fourier transform of  $h(t)$ . So the  $h(t)$  is

$$h(t) = \int_{-\infty}^{\infty} \left\{ \int_{-\infty}^{\infty} S(\tau, f) d\tau \right\} e^{j2\pi f t} df . \quad (2.9)$$

This shows that the concept the  $S$  transform is different from the CWT.

The relation between the  $S$  transform and Fourier transform can be written as

$$S(\tau, f) = \int_{-\infty}^{\infty} H(\alpha + f) e^{-\frac{2\pi^2 \alpha^2}{f^2}} e^{j2\pi \alpha \tau} d\alpha \quad f \neq 0. \quad (2.10)$$

By taking the advantage of the efficiency of the Fast Fourier transform and the convolution theorem, the discrete analog of (2.10) can be used to compute the discrete

$S$  transform (we will describe it below). If not translating the cosinusoid basic functions, the  $S$  transform can localize the real and imaginary components of the spectrum independently.

## 2.2 The Instantaneous Frequency

We set the 1-D function of the variable  $\tau$  and fixed parameter  $f_1$  as  $S(\tau, f_1)$  and called “voice”. Then the function can be written as

$$S(\tau, f_1) = A(\tau, f_1)e^{j\Phi(\tau, f_1)} \quad (2.11)$$

where  $A$  and  $\Phi$  are the amplitude and phase. Because a voice isolates a particular frequency  $f_1$ , we can use the phase  $\Phi$  to determine the instantaneous frequency (IF):

$$IF(\tau, f_1) = \frac{1}{2\pi} \frac{\partial}{\partial \tau} \{2\pi f_1 \tau + \Phi(\tau, f_1)\}. \quad (2.12)$$

The correctness of (2.11) can use a simple case of  $h(t) = \cos(2\pi\omega t)$ , where the function  $\Phi(\tau, f) = 2\pi(\omega - f)\tau$ .

## 2.3 The Discrete S Transform

Let  $h[kT]$ ,  $k=0, 1, \dots, N-1$  denote a discrete time series corresponding to  $h(t)$  with a time sampling interval of  $T$ . The discrete Fourier transform is shown as

$$H\left[\frac{n}{NT}\right] = \frac{1}{N} \sum_{k=0}^{N-1} h[kT] e^{-\frac{j2\pi nk}{N}}. \quad (2.13)$$

Using (2.10) and (2.13), the discrete time series  $h[kT]$ 's  $S$  transform is shown as (making  $f \rightarrow n/NT$  and  $\tau \rightarrow jT$ )

$$S\left[jT, \frac{n}{NT}\right] = \sum_{m=0}^{N-1} H\left[\frac{m+n}{NT}\right] e^{-\frac{2\pi^2 m^2}{n^2}} e^{-\frac{j2\pi m j}{N}} \quad n \neq 0 \quad (2.14)$$

where  $j, m,$  and  $n = 0, 1, \dots, N-1$ . If  $n = 0$  voice, it is equal to the constant defined as

$$S[jT, 0] = \frac{1}{N} \sum_{m=0}^{N-1} h\left(\frac{m}{NT}\right). \quad (2.15)$$

This equation makes the constant average of the time series into the zero frequency voice, so it will ensure that the inverse is exact. The inverse of the discrete  $S$  transform is

$$h[kT] = \sum_{n=0}^{N-1} \left\{ \frac{1}{N} \sum_{j=0}^{N-1} S\left[jT, \frac{n}{NT}\right] \right\} e^{-\frac{j2\pi nk}{N}}. \quad (2.16)$$

## 2.4 Self-Aliasing

Before clarifying the self-aliasing, we introduce “voice Gaussian” first. The voice Gaussian is the Fourier spectrum of the Gaussian window at a specific  $n$ . From (2.14), any voice of the S transform can be computed as the product of the Fourier spectrum  $H[m/NT]$  of the time series and the voice Gaussian. As we can see in (2.14), the voice Gaussian is

$$G(m, n) = e^{-\frac{m^2}{2(\frac{n}{2\pi})^2}}. \quad (2.17)$$

We have known that the discrete spectrum is periodic because sampling in the time domain. Thus, the self-aliasing occurs when  $n/NT$  approached the Nyquist frequency  $1/2T$ , the voice Gaussian overlaps into the negative frequencies of  $H[m/NT]$  or when the voice Gaussian becomes quite wide at high frequencies. For the sake of minimizing the effect of self-aliasing, the first method is that we define a special Nyquist frequency for the S transform as  $s_N$ . As the voice Gaussian is centered over  $s_N$ , the  $2\sigma$  point is at the Fourier Nyquist frequency  $f_N$ . It can write as

$$s_N + 2\frac{s_N}{2\pi} = f_N. \quad (2.18)$$

Consequently, the minimum sample rate  $T_s$  is

$$T_s = \frac{\pi + 1}{2\pi f_N}. \quad (2.19)$$

The second method is using the analytic signal of the time series for localization and then all negative frequencies will be set to zero [2]. Thus, there is no self-aliasing.

## 2.5 The simulate analysis

In this section, we discuss the simulation result from [1]. To show the class of time series for which the  $S$  transform would be useful.

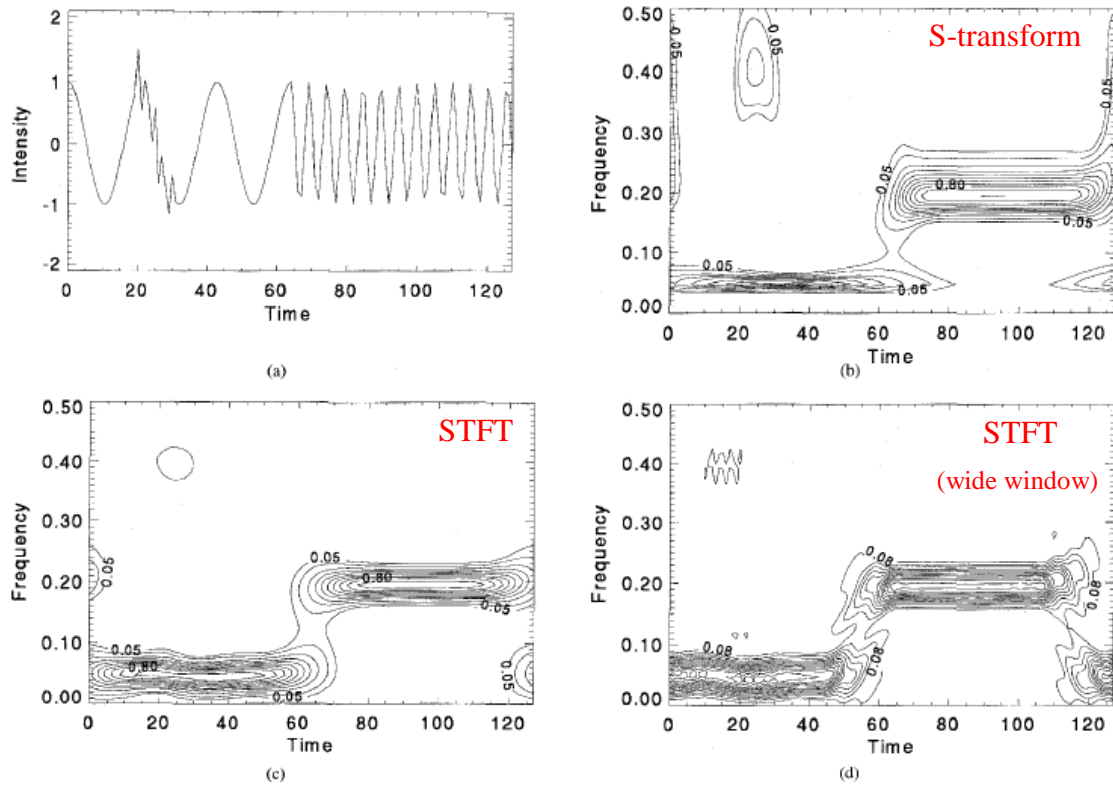


Fig. 2.1 (a) Synthetic time series composing of three different frequency signals; (b) amplitude of the  $S$  transform from the time series of Fig. 2.1(a); (c) amplitude of the short-time Fourier transform (STFT) from the time series of Fig. 2.1(a) using a fixed Gaussian window; (d) the same as Fig. 2.1(c), but change to the wider window size. [1]

In Fig. 2.1, (a) is a time series composing of high and low frequencies and a high-frequency burst which is used to compare the performance of the  $S$  transform and the STFT. Compare (b) with (c), we can see that on the low frequency signal, the  $S$  transform shows better frequency resolution than the STFT, however in the high frequency part, the resolution of the  $S$  transform is worse than the STFT. But observing the time resolution, the  $S$  transform can detect the occurred time and its energy variance of the high-frequency burst. Furthermore, from (c) and (d), the STFT has a tradeoff between detecting short-lived high-frequency signals and low-frequency signals. And while the window width of the STFT rises, it shows the poorly distinguishability of three signal components.

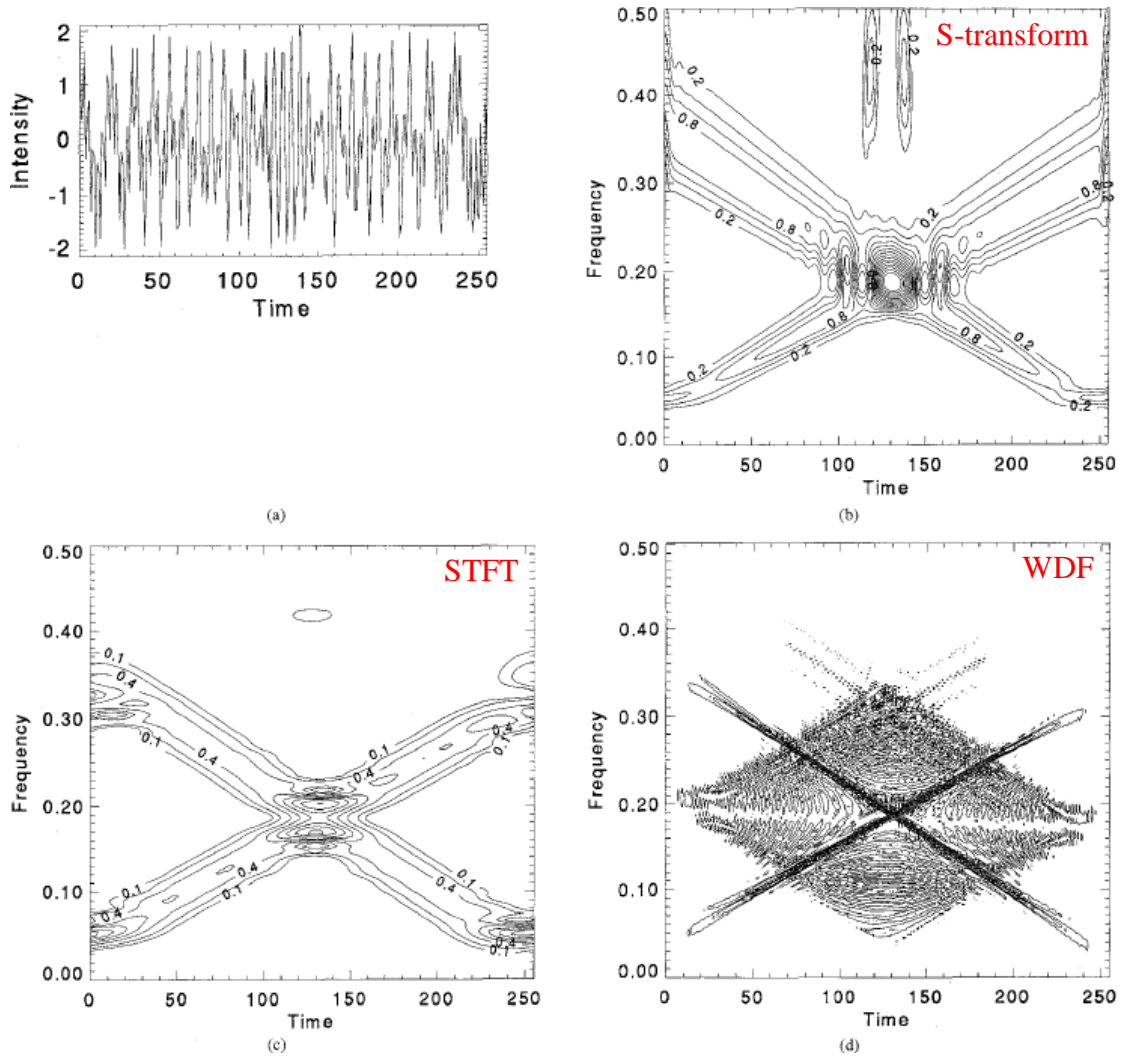


Fig. 2.2 (a) Synthetic time series composing of two high-frequency bursts and two cross chirps; (b) amplitude of the  $S$  transform from the time series of Fig. 2.2(a); (c) amplitude of the STFT (with Gaussian window) from the time series of Fig. 2.2(a); (d) amplitude of the Wigner distribution function from the time series of Fig. 2.2(a). [1]

In Fig. 2.2, (a) is a time series composing of two high-frequency bursts and two cross chirps. From (b), all four components can be detected by the  $S$  transform. In (c), the STFT can only detect the chirps, but cannot detect the high-frequency bursts. (d) shows the result of the Wigner distribution function (WDF), we can see that the WDF has good time and frequency resolution on the cross chirps. But the drawback is the WDF has cross terms, which will produce lots of part we do not want (represent noise). Moreover, the cross terms will cause the two bursts to be absolutely misrepresented.

### 3. Generalized $S$ Transform

#### 3.1 The Generalized $S$ Transform

The generalized  $S$  transform is defined as [3]

$$S(\tau, f, p) = \int_{-\infty}^{\infty} h(t)\omega(\tau-t, f, p)e^{-j2\pi ft} dt \quad (3.1)$$

where  $p$  denotes a set of parameters which determine the shape and properties of  $w$  and  $w$  denotes the  $S$  transform window shown as

$$\omega(t, f, p) = \frac{|f|}{\sqrt{2\pi p}} e^{-\frac{t^2 f^2}{2p^2}} \quad (3.2)$$

As (2.10), the generalized  $S$  transform can also be obtained by the Fourier transform given by

$$S(\tau, f, p) = \int_{-\infty}^{\infty} H(\alpha + f)W(\alpha, f, p)e^{j2\pi \alpha \tau} d\alpha \quad (3.3)$$

The  $S$  transform window  $w$  has to satisfy four conditions. The four conditions are as below

$$\int_{-\infty}^{\infty} \Re\{\omega(\tau, f, p)\}d\tau = 1, \quad (3.4)$$

$$\int_{-\infty}^{\infty} \Im\{\omega(\tau, f, p)\}d\tau = 0, \quad (3.5)$$

$$\omega(\tau-t, f, p) = [\omega(\tau-t, -f, p)]^*, \quad (3.6)$$

$$\frac{\partial}{\partial t} \Phi(\tau-t, f, p)\Big|_{t=\tau} = 0. \quad (3.7)$$

The first two conditions assure that when integrated over all  $\tau$ , the  $S$  transform converges to the Fourier transform:

$$\int_{-\infty}^{\infty} S(\tau, f, p)d\tau = H(f). \quad (3.8)$$

The third condition can ensure the property of symmetry between the shapes of the  $S$  transform analyzing function at positive and negative frequencies.

#### 3.2 The Gaussian Window

Before introducing the bi-Gaussian window, we first mention the Gaussian window. As we can see in (3.2),  $\omega$  is a Gaussian. To difference Gaussian window from the bi-Gaussian, we use the subscript  $GS$  to represent (3.2)'s modification.  $\omega_{GS}$  is

rewritten as [4]

$$\omega_{GS}(\tau - t, f, \{\gamma_{GS}\}) = \frac{|f|}{\sqrt{2\pi}\gamma_{GS}} e^{-\frac{f^2(\tau-t)^2}{2\gamma_{GS}^2}} \quad (3.9)$$

where  $\gamma_{GS}$  is the number of periods of Fourier sinusoid which are contained within one standard deviation of the Gaussian window. We show the Gaussian  $S$  transform of the time series for  $\gamma_{GS} = 1$  in Fig. 3.1. The result of Fig. 3.1 is obtained by using the discrete  $S$  transform (2.14), shown as  $S_{GS}$ . In order to get  $S_{GS}$ , we have to obtain  $W_{GS}$  first.  $W_{GS}$  is shown as

$$W_{GS}(\alpha, f, \{\gamma_{GS}\}) = e^{-\frac{2\pi^2\alpha^2\gamma_{GS}^2}{f^2}}. \quad (3.10)$$

From Fig. 3.1, there has a problem that the long front taper of the window let the correlation of event signatures with the time of event initiation be complex.

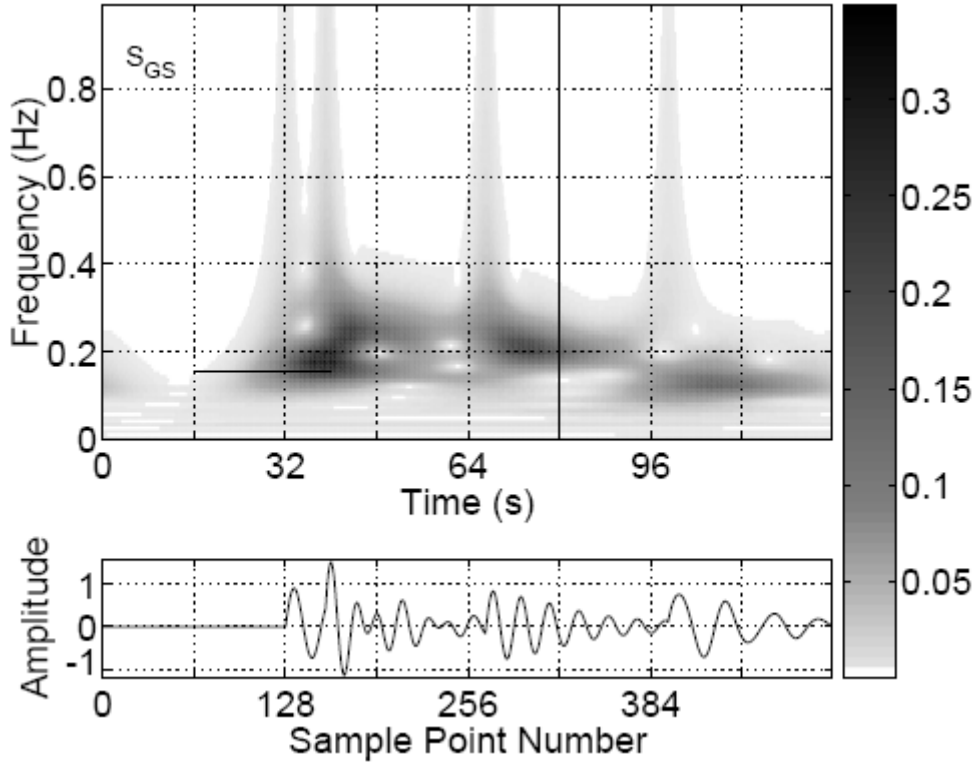


Fig. 3.1 The time series and the amplitude spectrum of Gaussian  $S$  transform of time series at  $\gamma_{GS} = 1$ . From the event signatures, we can see the “holes”, which is due to localized destructive interference between signal components. [4]

In order to improve the front time resolution of  $\omega_{GS}$ , we can decrease the value of  $\gamma_{GS}$  for narrowing the window. However, a drawback is that if  $\gamma_{GS}$  is too small, the window may reserve too few cycles of the sinusoid. So the frequency resolution may be poor and may let the time-frequency spectrum be meaningless. There is an example in Fig. 3.2.

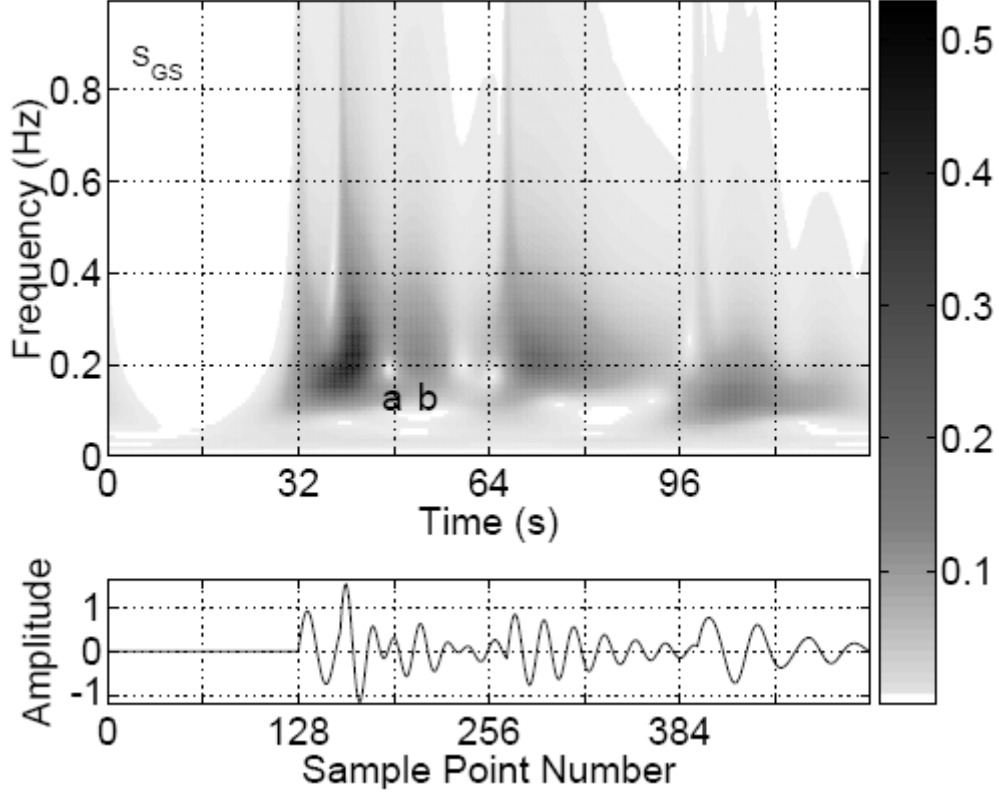


Fig. 3.2 The time series and the amplitude spectrum of Gaussian  $S$  transform of time series at  $\gamma_{GS} = 0.5$ . “a” is the position that has destructive localized interference between two events and “b” is a phantom fifth event between second and third real events. [4]

### 3.3 The Bi-Gaussian Window

The more appropriate method is use an asymmetric window with a decreased front taper and an increased back taper. The decreased front taper may improve the resolution of event initiation time and the increased back taper improves the resolution in frequency domain. The disadvantage is that the resolution of event termination time will be worse, but fortunately many applications do not pay attention on event termination time.

The good asymmetric window is the bi-Gaussian window  $\omega_{BG}$ , which is constructed by two different half Gaussians with different tapers in the front and back directions. There is a diagram shown the difference between the Gaussian and bi-Gaussian window. The expression of  $\omega_{BG}$  is given by [4]

$$\omega_{BG}(\tau - t, f, \{\gamma_{BG}^B, \gamma_{BG}^F\}) = \frac{|f|}{\sqrt{2\pi}} \frac{2}{(\gamma_{BG}^B + \gamma_{BG}^F)} e^{-\frac{f^2(\tau-t)^2}{2[\gamma_{BG}^B(\tau-t)]^2}} \quad (3.11)$$

where

$$\begin{aligned}\tilde{\gamma}_{BG}(\tau-t) &= \gamma_{BG}^B, & t \geq \tau \\ &= \gamma_{BG}^F, & t < \tau.\end{aligned}\quad (3.12)$$

The taper of the back half Gaussian is the case of  $t \geq \tau$ , the taper of a full Gaussian's standard deviation is equal to  $\gamma_{BG}^B$ , called the back taper parameter. The taper of the front half Gaussian is the case of  $t < \tau$ , the taper of a full Gaussian's standard deviation is equal to  $\gamma_{BG}^F$ , called the front taper parameter. The Fourier transform of  $\omega_{BG}$  is shown as (it contains the error function  $erf$  (see [5, p. 483]))

$$\begin{aligned}W_{BG}(\alpha, f, \{\gamma_{BG}^B, \gamma_{BG}^F\}) &= \left( \frac{1}{\gamma_{BG}^B + \gamma_{BG}^F} \right) \\ &\times \left\{ \gamma_{BG}^B e^{-\frac{2\pi^2\alpha^2(\gamma_{BG}^B)^2}{f^2}} \left[ 1 + erf\left(\frac{j\sqrt{2\pi}\alpha\gamma_{BG}^B}{|f|}\right) \right] \right. \\ &\left. + \gamma_{BG}^F e^{-\frac{2\pi^2\alpha^2(\gamma_{BG}^F)^2}{f^2}} \left[ 1 - erf\left(\frac{j\sqrt{2\pi}\alpha\gamma_{BG}^F}{|f|}\right) \right] \right\}.\end{aligned}\quad (3.13)$$

In order to control the time dispersion of the whole window, PINNEGAR and MANSINHA represent  $\omega_{BG}$  in terms of  $\gamma_{BG}^F$  and a width parameter similar to  $\gamma_{GS}$ , denoted  $\gamma_{BG}$ . Then  $\gamma_{BG}^B$  is defined in terms of  $\gamma_{BG}$  and  $\gamma_{BG}^F$  as below.

$$\gamma_{BG}^B = \frac{(\pi-4)}{2(\pi-2)}\gamma_{BG}^F + \frac{\sqrt{(8\pi-3\pi^2)(\gamma_{BG}^F)^2 + (4\pi^2-8\pi)\gamma_{BG}}}{2(\pi-2)}.\quad (3.14)$$

There is a diagram shown the difference between the Gaussian and the bi-Gaussian windows in time domain in Fig. 3.3 and the example of bi-Gaussian  $S$  transform of the time series in Fig. 3.4.

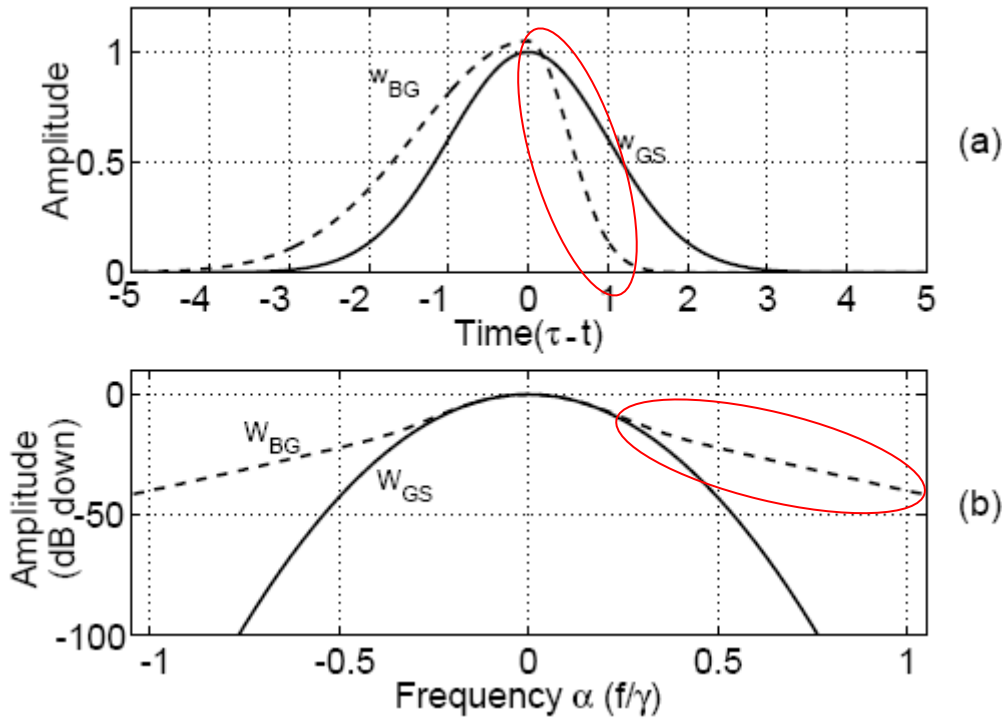


Fig. 3.3 (a) The Gaussian and bi-Gaussian windows in time domain. The solid and dashed lines denote  $\omega_{GS}$  and  $\omega_{BG}$ , respectively (both have the same frequency). See the region of red circle of  $\omega_{BG}$ , it is the part of the front half Gaussian ( $t < \tau$ ) and we adjust  $\gamma_{BG}^F$  to be small. Then as we can see, the shape of the line is sharper at arrival time. That means the time resolution will become better, but the frequency resolution will become worse. This advances the efficiency of detecting the earthquake occurrence instantaneously. (b) The Gaussian and bi-Gaussian windows in frequency domain. The solid and dashed lines denote  $\omega_{GS}$  and  $\omega_{BG}$ , respectively (both have the same frequency). This proves the theorem of the frequency resolution will become worse when  $\tilde{\gamma}_{BG}(\tau - t)$  is small. But for the detection of earthquake occurrence, it is not important to know its frequency at time  $< 1$  second. [4]

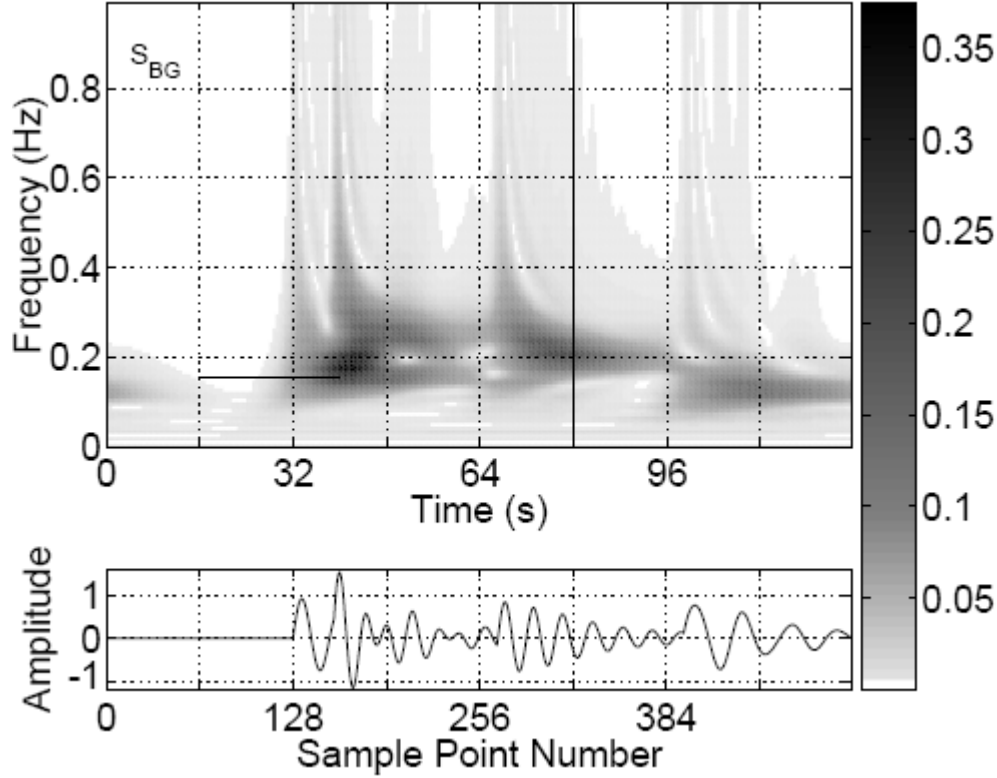


Fig. 3.4 The time series and the amplitude spectrum of Gaussian  $S$  transform of time series at  $\gamma_{BG} = 1$  and  $\gamma_{BG}^F = 0.5$ . Compare to Fig. 3.2, the time resolution of event initiations is approximately same because the front taper of the Gaussian window and the front taper of the bi-Gaussian window are similar. But the frequency resolution is much likely to Fig. 3.1 because the Gaussian window's time dispersion is similar with bi-Gaussian window at all  $n$ . Although the interference “holes” are asymmetrical, they are easier to discriminate than the “holes” in Fig. 3.2. [4]

## 4. Seismic Waves Analysis

### 4.1 The Hyperbolic Window

To identify the time-frequency signatures of seismic wave trains, there is another asymmetrical window called the “hyperbolic” window proposed from [6]. The hyperbolic window  $\omega_{HY}$  is a pseudo-Gaussian. PINNEGAR and MANSINHA obtain  $\omega_{HY}$  from the generalized window (from (3.1)) by replacing  $\omega$  with

$$\omega_{HY} = \frac{2|f|}{\sqrt{2\pi}(\gamma_{HY}^F + \gamma_{HY}^B)} e^{-\frac{f^2 [X(\tau-t, \{\gamma_{HY}^B, \gamma_{HY}^F, \lambda_{HY}^2\})]^2}{2}} \quad (3.15)$$

where

$$X\left(\tau-t, \left\{\gamma_{HY}^B, \gamma_{HY}^F, \lambda_{HY}^2\right\}\right) = \left(\frac{\gamma_{HY}^B + \gamma_{HY}^F}{2\gamma_{HY}^B \gamma_{HY}^F}\right)(\tau-t-\zeta) + \left(\frac{\gamma_{HY}^B - \gamma_{HY}^F}{2\gamma_{HY}^B \gamma_{HY}^F}\right) \sqrt{(\tau-t-\zeta)^2 + \lambda_{HY}^2}. \quad (3.16)$$

In equation (3.16),  $X$  is a hyperbola in  $(\tau - t)$  and depends on a back taper parameter  $\gamma_{HY}^B$ , a front taper parameter  $\gamma_{HY}^F$  (assume  $0 < \gamma_{HY}^F < \gamma_{HY}^B$ ), and a positive curvature parameter  $\lambda_{HY}$ .  $\zeta$  is the purpose of assuring the peak of  $\omega_{HY}$  occurs at  $(\tau - t) = 0$ ,  $\zeta$  is defined as

$$\zeta = \sqrt{\frac{(\gamma_{HY}^B - \gamma_{HY}^F)^2 \lambda_{HY}^2}{4\gamma_{HY}^B \gamma_{HY}^F}}. \quad (3.17)$$

There is a diagram shown the hyperbolic window in Fig. 4.1 with  $\gamma_{HY}^B = 1.5$ ,  $\gamma_{HY}^F = 0.5$ , and  $\lambda_{HY}^2 = 1$ . We can see that when  $f$  tend to zero,  $\omega_{HY}$  becomes very asymmetrical and as  $f$  increases, the shape of  $\omega_{HY}$  converges to resemble symmetric window ( $\omega_{GS}$ ).

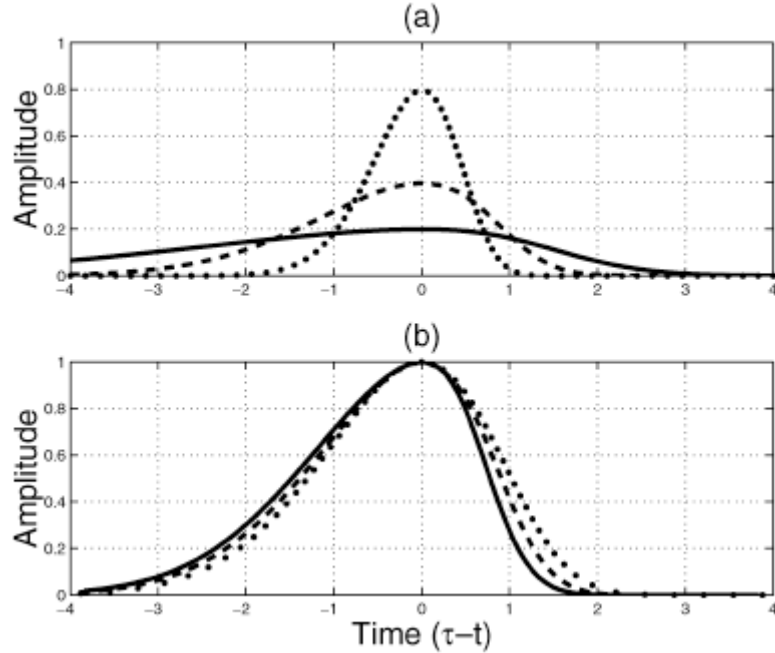


Fig. 4.1 (a) Hyperbolic window  $\omega_{HY}$  at  $f = 0.5$  (solid line),  $f = 1$  (dashed line), and  $f = 2$  (dotted line), with  $\gamma_{HY}^B = 1.5$ ,  $\gamma_{HY}^F = 0.5$ , and  $\lambda_{HY}^2 = 1$ . (b) Let three windows through the horizontal dilation to deviation of 1 and the vertical dilation to a maximum

height of 1 because the difference of  $f$  makes the frequency dependent asymmetry of  $\omega_{HY}$  difficult to distinguish visually in Fig. 4.1 (a). [6]

## 4.2 The Result of the $S$ Transform of Seismogram

In this section, we show some analysis charts from [6]. Fig. 4.2 is the extraction of the seismogram by using a 400-point segment (from 5 to 8.99s) and its Gaussian  $S$  transform with  $\gamma_{GS} = 1$ . The original seismogram is a 20s segment of the north-south component of an earthquake noisy seismogram. From Fig. 4.2, we can see that there is an increase in frequency at 6.73s in the time series. It is the arrived time of the P-wave. Nevertheless, its  $S$  transform shows that the real P-wave's arrived time occurs later than 6.73s. The reason of the wrong arrived time in time series is that there is a local increase in the amplitude of the 12Hz noise.

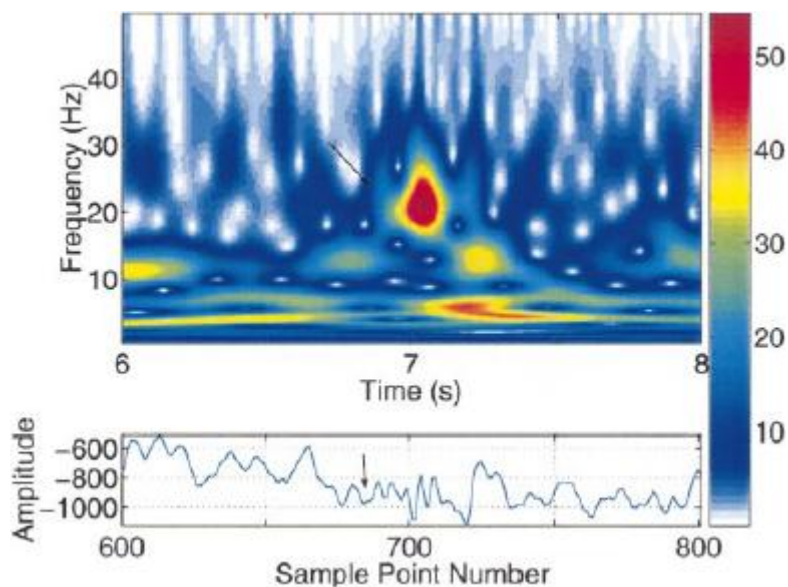


Fig. 4.2 A segment of the noisy earthquake seismogram and its Gaussian  $S$  transform with  $\gamma_{GS} = 1$ . The arrived time of the P-wave is marked with an arrow on the time series and the time-frequency domain. The time-frequency signatures present clearly on the  $S$  transform, but not easily discern on the time trace. [6]

Fig. 4.3 is similar to Fig. 4.2, but use the hyperbolic window to run the  $S$  transform. We can see that the time-frequency signature of the P-wave arrival in Fig. 4.3 has a more “vertical” contour than Fig. 4.2.

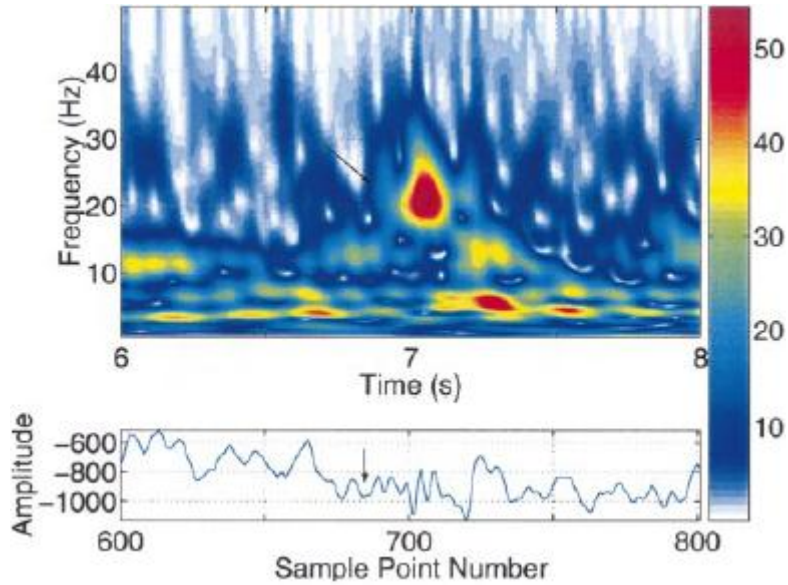


Fig. 4.3 A segment of the noisy earthquake seismogram and its hyperbolic  $S$  transform with  $\gamma_{HY}^B = 1.5$ ,  $\gamma_{HY}^F = 0.5$ , and  $\lambda_{HY}^2 = (1/16)^2$ . [6]

After the position of the event has been determined, PINNEGAR and MANSINHA use the time-frequency filter [6] to get the part of the P-wave initiation from Fig. 4.3 and use the inverse  $S$  transform to know the real P-wave arrival, which is the sharper positive peak at 6.86s shown on Fig. 4.4.

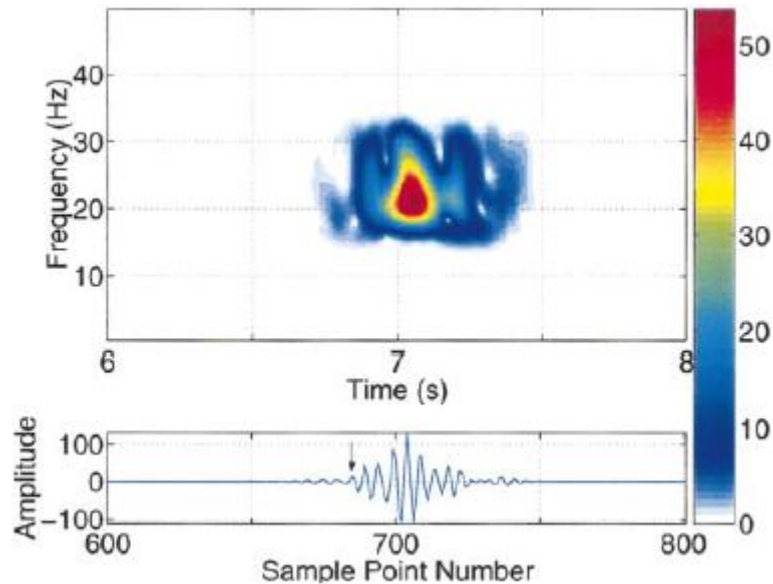


Fig. 4.4 The  $S$  transform of Fig. 4.3 after the time-frequency filter designed to reserve the P-wave event signature and the time series after the inverse  $S$  transform. The real P-wave arrival is marked with an arrow at 6.86s. [6]

## 5. Analysis of Engine Induction Noise in Acceleration

According to the engine motion principle, the pressure fluctuation will cause the induction noise when the intake valve is opened or closed periodically. The lower frequencies correlated with the basic frequency of rotation may dominate the periodic induction noise signals. The predominant frequency is defined as [7]

$$f_0 = v \frac{zn}{30\tau} \quad (5.1)$$

where  $n$  is the engine speed,  $z$  and  $\tau$  is the number of cylinder and stroke, respectively, and  $v$  is the order. Then we can know the predominant frequency of induction noise increases with engine speed linearly from (5.1).

We show the example of the noise signal acquired on a four cylinder engine stalled in a semi-anechoic laboratory from [7]. This engine works at half-load and the speed accelerates from 1260 to 5550 r/min steadily. Fig. 5.1 shows the engine speed and the fundamental frequency curve of induction noise. First, Zhang and et al. list the predominant frequencies of engine induction noise corresponding to different speed phases as follows: 42~48Hz, 48~58Hz, 58~75Hz, 75~87Hz, 87~110Hz, 110Hz~120Hz, 120~150Hz, 150~160Hz, 160~170Hz and 170~185Hz.

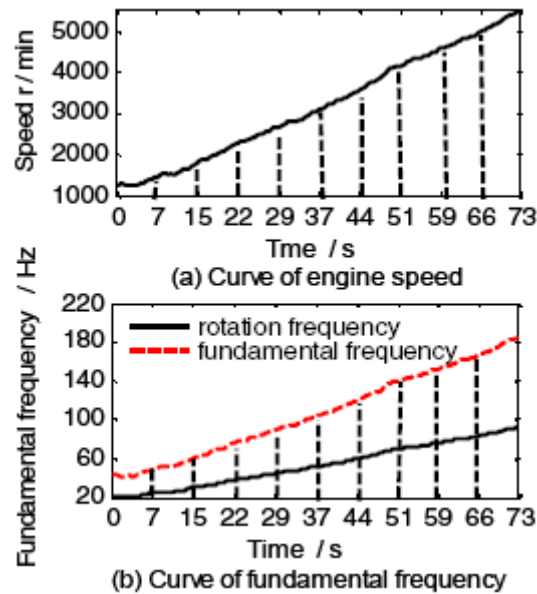


Fig. 5.1 The engine speed and the fundamental frequency curve of induction noise. [7]

Fig. 5.2 presents the  $S$  transform results of the engine induction noise. The higher shade level represents the greater energy intensity. Fig. 5.2(a) ~ 5.2(c) show the  $S$  transform results of the first three data segments. All of them show the characteristic of higher concentration in time-frequency domain and their linearly modulated frequency totally distribute in the range of 42~48Hz, 48~58Hz, and 58~75Hz.

Moreover, their shade level of linearly modulated frequency band decreases when the engine speed increases. As we can see in Fig. 5.2 (c), the shade level of linearly modulated frequency band decreases to the lowest when speed comes to 2200 r/min. It is consistent with the fundamental frequency curve of engine induction noise in the speed range of 1260 to 2250 r/min in Fig 5.1 (b).

Fig. 5.2(d) ~ 5.2(g) show the  $S$  transform results of the next four data segment. Not as the first three segments, the four signal energy do not only concentrate on the four linearly modulated frequency bands defined by 75~87Hz, 87~110Hz, 110Hz~120Hz, and 120~150Hz, but also randomly distributed in other frequency bands. Especially in Fig. 5.2 (f) and (g), their energy distributions are more extensive in other frequency bands. That represents after the velocity exceeds 2250 r/min, the energy distribution of induction noise become more and more extensive with the raise of engine speed.

Fig. 5.2(h) ~ 5.2(j) show the  $S$  transform results of the last three data segment. As Fig. 5.2(d) ~ 5.2(g), these three segments also include lots of frequency components and have higher concentration on the linearly modulated frequency bands defined by 150~160Hz, 160~170Hz, and 170~185Hz. Take notice that the amplitude of noise signal increases with engine speed, especially after the velocity exceeds 5100 r/min (68s), the upward trend of the amplitude is much more remarkable.

There is the red dashed line in Fig. 5.2(a) ~ 5.2(j), that is the connection of the starting frequency and the terminal frequency of each linearly modulated frequency band. It shows that the red dashed line is agreement with the fundamental frequency curve of engine induction noise shown in Fig. 5.1(b).

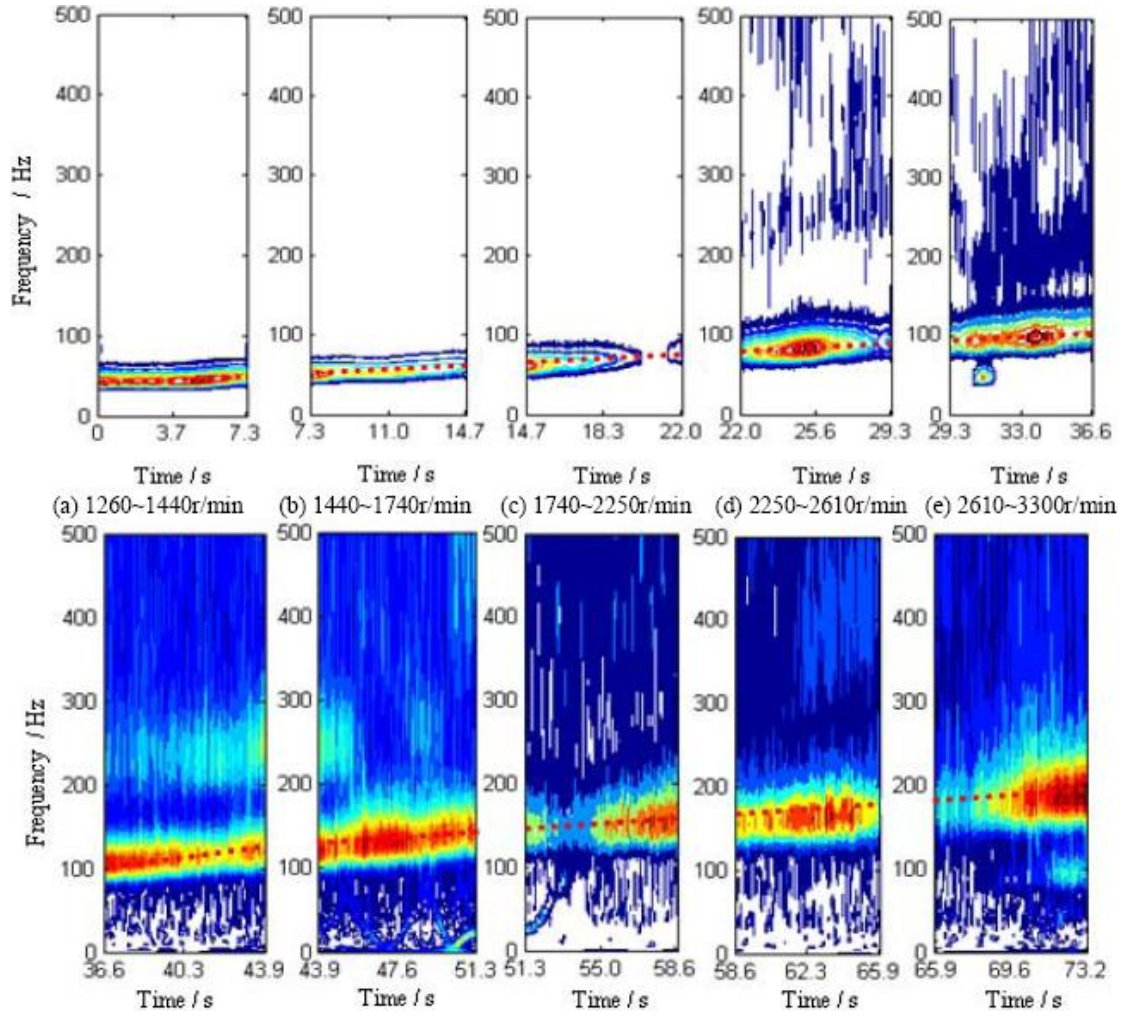


Fig. 5.2 The  $S$  transform results of the engine induction noise in acceleration. [7]

## 6. Power Quality Analysis

The power quality (PQ) includes voltage sag, swell, interruption, oscillatory transients, spike, notch, harmonics, and harmonics with sag, harmonics with swell and harmonics with interruption. Then we will display the  $S$  transform and the WT of voltage sag, swell, spike, oscillatory transients, and harmonic in following from [8].

Fig. 6.1(a) shows the case of consecutive voltage sags and swells with the noise signal. Fig. 6.1(b) is the curve of normalized frequency corresponding to the magnitude of the frequency components. Normalized frequency is given by [9]

$$f_n = nf_0 / f_s, \quad n = 1, 2, 3, \dots \quad (6.1)$$

where  $f_0$  is fundamental frequency (50Hz),  $f_s$  is sampling frequency (2 kHz). Fig. 6.1(c) is the plot of RMS (Root Mean Square) values of the signal versus samples. The RMS values are acquired from the maximum amplitudes of the  $S$  transform matrix at every sampling, the formula is given by [8]

$$\left| S \left[ jT, \frac{n}{NT} \right] \right|. \quad (6.2)$$

Fig. 6.1(d) is the plot of performing the WT using db4 wavelet. Compare Fig. 6.1(c) and (d), we can know that when there is noise in the signal, the WT cannot identify the sag/swell condition, but S transform has ability to detect the occurrence of noise disturbance correctly.

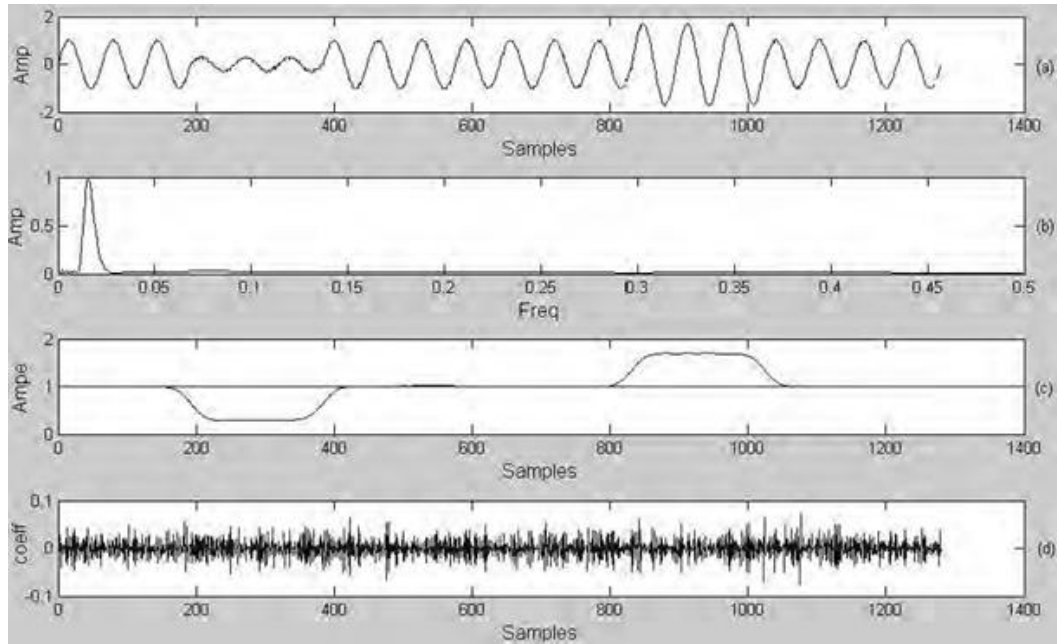


Fig. 6.1 Voltage sags and swells with the noise signal. [8]

Fig. 6.2 is similar to Fig. 6.1. It shows the S transform detects voltage spike and oscillatory transients successfully and effectively. Nevertheless, the WT fails to recognize the oscillatory transient condition.

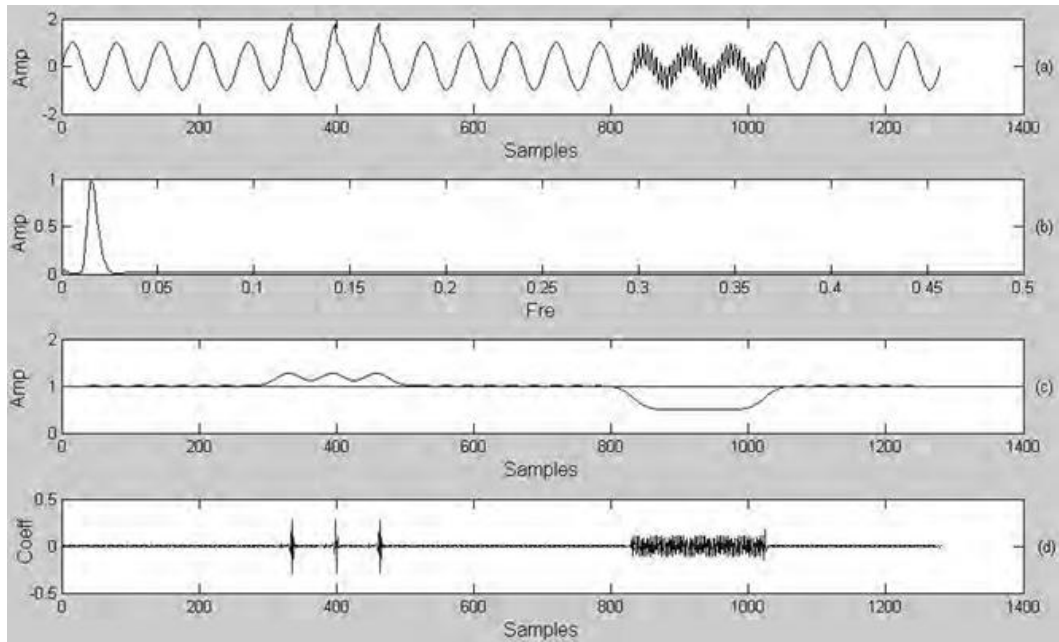


Fig. 6.2 Voltage spike and oscillatory transients. [8]

Fig. 6.3(a) and 6.4(a) show the harmonic signal and harmonic signal with voltage sag and swell. We can see that the harmonic signal and the signal with harmonic will have other frequency component except the fundamental frequency from Fig. 6.3(b) and 6.4(b). Fig. 6.4(c) reveals the S transform can exactly detect the voltage sag and swell from disturbances with harmonic. However, Fig. 6.4(d) shows the WT may be influenced by harmonic.

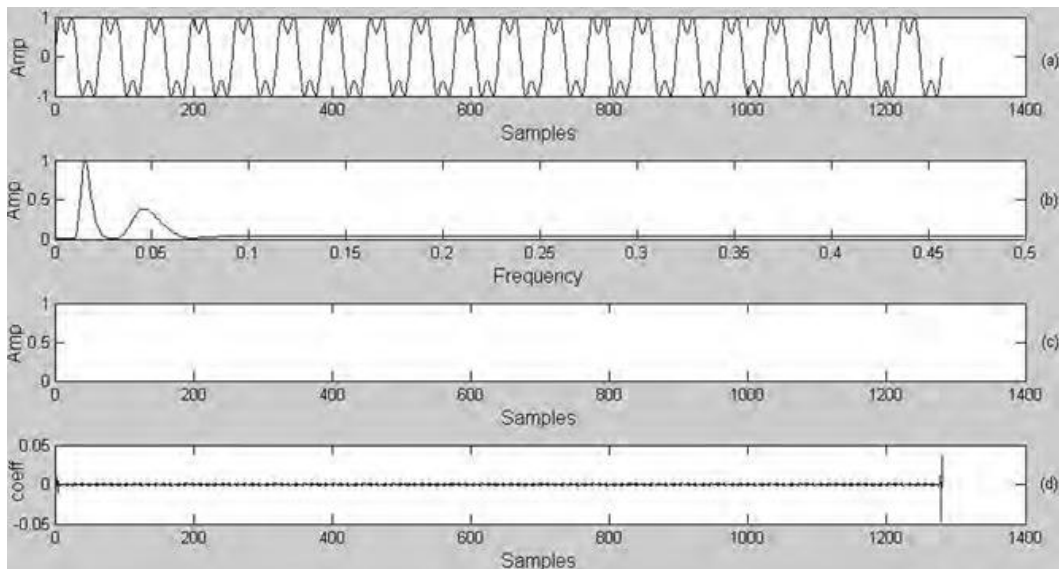


Fig. 6.3 Voltage harmonic signal. [8]

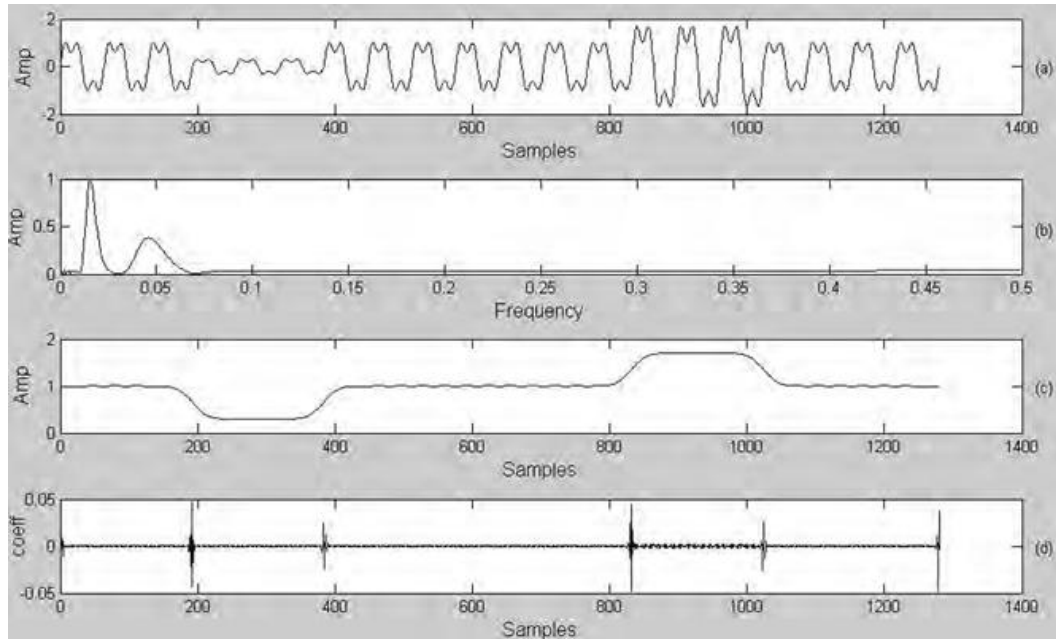


Fig. 6.4 Voltage harmonic with sag and swell. [8]

## 7. Conclusion

We have shown the concept of the transform between the S transform and the STFT, WT. In the extension, present the generalized S transform, which its application of windows having frequency dependence in their shape (width and height). For the different applications, we can choose the suitable window and parameters to acquire the good resolution in the part we want to emphasize. From the power quality analysis, the S transform exhibit the ability of identifying the power quality disturbance by noise or transient. This is the wavelet transform cannot achieve because its drawback of sensitive to noise. But the S transform still have two drawbacks, first one is in the DC term (frequency = 0), the S transform cannot analyze the variation of S transform on time. Second, in high frequency, the window will be too narrow, so the points we can practically apply will be too less.

Except the applications of S transform we present in this tutorial, there are numerous applications which is suitable for the S transform such as heart sound analysis, image watermarking, filter design, etc.

## Reference

- [1] R. G. Stockwell, L Mansinha and R P Lowe, "Localization of the complex spectrum: The S Transform," *IEEE Trans. Signal Processing*, vol. 44, no. 4, pp. 998-1001, April. 1996.

- [2] B. Boashash, "Notes on the use of the wigner distribution for time-frequency signal analysis," *IEEE Trans. Acoust. Speech, Signal Processing*, vol. ASSP-35, no. 9, Sept. 1987.
- [3] C. R. Pinnegar, L. Mansinha, "Time-local Fourier analysis with a scalable, phase-modulated analyzing function: the  $S$ -transform with a complex window," *Signal Processing*, vol. 84, pp. 1167-1176, July. 2004
- [4] C. R. Pinnegar, L. Mansinha, "The Bi-Gaussian  $S$  transform," *SIAM J. SCI. COMPUT.*, vol. 24, no. 5, pp. 1678-1692, 2003.
- [5] I. S. Gradshteyn and I. M. Ryzhik, *Table of Integrals, Series and Products*, 6th ed., Academic Press, New York, 2000.
- [6] C. R. Pinnegar, L. Mansinha, "The  $S$ -transform with window of arbitrary and varying shape," *GEOPHYSICS*, vol. 68, no. 1, pp. 381-385, 2003.
- [7] HAO Z., XU H., ZHENG G., JING G., "Study on the Time-frequency Characteristics of Engine Induction Noise in Acceleration Based on  $S$  Transform," *IEEE CISP*, vol. 5, pp.242-246, 2008
- [8] Zhang S., Liu R., Wang Q., J. T. Heptol, Yang G., "The Research of Power Quality Analysis Based on Improved  $S$ -Transform," *IEEE ICEMI'2009*, vol. 9, pp. 2-477 – 2-481, Aug. 2009.
- [9] C. Venkatesh, D.V.S.S. Siva Sarma, M. Sydulu, "Detection of Voltage Sag/Swell and Harmonics Using Discrete  $S$ -Transform". *IEEE transactions on power delivery*, vol. 15, no. 1, pp. 247-253, JAN. 2000.